

A Disposable Haptic Palpation Probe for Locating Subcutaneous Blood Vessels in Robot-Assisted Minimally Invasive Surgery

Stephen McKinley¹, Animesh Garg², Siddarth Sen³, Rishi Kapadia³, Adithyavairavan Murali³, Kirk Nichols⁴, Susan Lim⁵, Sachin Patil³, Pieter Abbeel³, Allison M. Okamura⁴, Ken Goldberg²

Abstract—We present the design and evaluation of a novel low-cost palpation probe for Robot assisted Minimally Invasive Surgery (RMIS) for localizing subcutaneous blood vessels. It measures probe tip deflection using a Hall Effect sensor as the spherical tip is moved tangentially across a surface under automated control. The probe is intended to be single-use and disposable, built from 3D printed parts and commercially available electronics. The prototype has a cross-section of less than $15\text{ mm} \times 10\text{ mm}$ and fits on the end of an 8mm diameter needle driver in the Intuitive Surgical da Vinci® Research Kit (dVRK). We report experiments for quasi-static sliding-mode palpation with silicone based tissue phantoms with embedded cylinders as subcutaneous blood vessel phantoms. We analyzed signal-to-noise ratios with multiple diameters of silicone cylinders ($1.58\text{-}4.75\text{ mm}$) at varying subcutaneous depths ($1\text{-}5\text{ mm}$) with a range of indentation depths ($0\text{-}8\text{ mm}$) and sliding speeds ($0.5\text{-}21\text{ mm/s}$). Results suggest that the probe can detect subcutaneous structures in phantoms of diameter 2.25 mm at a depth of up to 5 mm below the tissue surface.

I. INTRODUCTION

Robotic surgical assistants (RSAs) such as the Intuitive Surgical's da Vinci system have been shown to be effective in facilitating precise minimally invasive surgery [5, 32], by providing increased dexterity and control for the surgeon. In clinical usage, these devices are controlled by surgeons in local teleoperation mode (master-slave with negligible time delays) without haptic feedback. Tactile and force sensors have potential to provide haptic feedback enabling the surgeon to perform an array of survey operations such as in-situ diagnosis and localization.

During open surgery, a surgeon can directly palpate tissue allowing localization of a number of subcutaneous (external organ membrane) or subserous (internal organ membrane) inclusions based on changes in tissue reaction force relative to surrounding substrate (parenchyma) [33]. Even though robot-assisted minimally invasive surgery (RMIS) is frequently used in cancer surgeries [22], the lack of force perception in RMIS has been shown to increase tissue trauma and accidental tissue damage [6]. Williams et al. [34] show that the lack of tactile or force feedback in RMIS, as compared

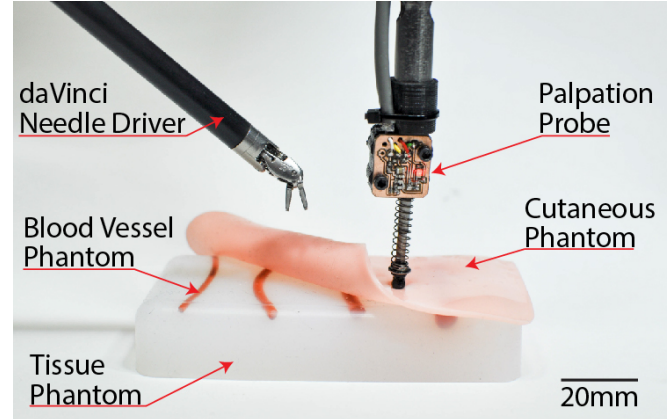


Fig. 1: A disposable palpation probe mounted on the tip of an 8 mm diameter dVRK needle driver tool is shown alongside a regular 8 mm diameter da Vinci tool and a with a tissue phantom with subcutaneous vessels. This device is a low-cost extension to an existing da Vinci tool for acquiring tactile information from surface probing in robot-assisted minimally invasive surgery.

to open surgery, can lead to increased likelihood of leaving behind target cells during debridement in a diseased region.

A recent survey of medical tactile force sensors by Konstantinova et al. [14] reports that numerous devices exist to estimate tactile information during static (point based) measurements. However, a gap exists in scanning soft tissue surfaces in a dynamic (continuous) manner. Another major limitation in clinical use of tactile force sensing in RMIS is the need for sterilization of tools [2]. After every use, end-effectors are cleaned in an autoclave using high-pressure, high-temperature steam. Most haptic sensors have delicate components, such as resistive strain gauges or electromagnets, which cannot withstand such a harsh sterilization process. Hence, there is a need to develop low-cost single-use tactile or force sensing devices for RMIS that operate in real-time, provide reproducible and repeatable measurements.

Contributions: We present a novel low-cost, disposable, haptic palpation probe to be used with the da Vinci RSA tools as shown in Figure 1. The probe is designed to sense relative deflection differences for localization of subcutaneous or subserous inclusions such as blood vessels or tumors. It is an indentation based device using a displacement-based contact sensing mechanism. A spherical indenter of 4.5 mm diameter allows quasi-static sliding palpation for continuous measurements analogous to human fingertip sensation.

We discuss the probe design details along with sliding-mode indentation experiments on silicone-based tis-

¹Mechanical Engineering, University of California, Berkeley; mckinley@berkeley.edu

²IEOR and EECS, University of California, Berkeley; {animesh.garg, goldberg}@berkeley.edu

³EECS, University of California, Berkeley; {siddarthsen, rishikapadia, adithya.murali, sachinpatil, pabbeel}@berkeley.edu

⁴Mechanical Engineering, Stanford University; {kirk.nichols, aokamura}@stanford.edu

⁵Centre for Breast Screening and Surgery, Centre for Robotic Surgery, Singapore; susanlim@berkeley.edu

sue phantoms. Silicone inclusions of varying diameters ($\{1.58, 2.38, 3.175, 4.75\}$ mm) placed at varying depths ($\{1, 2, 3, 5\}$ mm) were used to evaluate probe sensitivity. For characterization of robustness to sliding surface speed, the probe was mounted on a CNC milling machine (as shown in Figure 5) and was palpated across the tissue phantom in sliding-mode at varying indentation depths ($\{1, 3, 8\}$ mm) and sliding speeds (0.5–21 mm/s). We also demonstrate the use of the palpation probe as a tool mounted on the dVRK to perform automated sliding palpation in the silicone-based tissue phantoms. Initial results suggest a potential for the clinical utility of automated sliding palpation in both supervised and semi-supervised telesurgery.

II. BACKGROUND AND RELATED WORK

Tactile force sensing is used by humans to explore, manipulate, or respond to their environment [4]. Robotic tactile sensing is applied in diverse fields including surgical devices, industrial equipment, and dexterous robotic hands [4]. In this paper, we focus on the exploratory and diagnostic aspect of tactile feedback within the purview of RMIS.

Palpation sensors are a subclass of tactile and force sensors that mimic the biological sense of cutaneous touch. In RMIS, palpation sensors can estimate relative tissue stiffness and allow the surgeon to adjust force control input for safer tissue manipulation. It has been demonstrated that a RMIS tool equipped with tactile sensing under autonomous control reduces the maximum applied force to the tissue by more than 35% compared to manual palpation with the same instrument [31]. Other studies have compared human sensing with probing sensors for tumor localization and have found probing sensor arrays to be more effective in requiring lesser forces for inclusion identification [11, 26].

Methods of tactile force sensing: Tactile feedback can be obtained by using a number of transduction principles [14, 24]. We refer the reader to Girão et al. [9] and Tiwana et al. [30] for a detailed survey of existing tactile and force feedback devices in the context of robotic and biomedical applications respectively. Particularly, tactile sensing can be classified based on its underlying transduction principles: mechanical [7], piezoresistive [28], capacitive [27], piezoelectric [25], strain gauge [13], optical [21], and magnetic [29]. While each of these techniques has respective advantages and limitations as listed by Tiwana et al. [30], a number of the techniques require complicated signal conditioning infrastructures, are susceptible to drift, and have a limited range of measurable forces.

Existing tactile force sensors for RMIS: Konstantinova et al. [14] provide a survey of a number of RMIS tactile feedback devices and compare them based on desired features for tactile probes in RMIS such as: (a) repeatability, (b) reliability, (c) speed of sensing, (d) static versus dynamic response, (d) miniaturized form and (e) cost. Also, RMIS tools are between 5 mm to 12 mm in diameter [18], hence the sensor needs to be small enough to pass through the trocar port and be placed proximal to the tool-tip. Further, strict

certification requirements for medical devices warrant that these probes have high accuracy and stable response.

There have been a number of efforts in probe design research to address some of these considerations. Althoefer et al. [1] presented a sensor using compressed air to investigate the mechanical properties of soft tissue; maintaining constant air-flow is a challenge and requires additional equipment. Murayama et al. [19] devised a sensor array for lump detection in breast cancer aimed at identifying large (> 10 mm) inclusions close to the surface (< 20 mm) but it faces limited adoption in laparoscopic procedures given its large size (45 mm in cross-section). Beccani et al. [3] developed a wireless sensor based on external static magnetic fields within a small workspace. Developments in MEMS devices have allowed a multitude of sensors to be miniaturized inexpensively. Peng et al. [23] proposed a MEMS tactile sensor which can provide fast relative elasticity measurement. Gafford et al. [8] proposed a monolithic approach to build a tri-axis force sensor for medical applications. However, none of these methods provide continuous tangential sliding-mode surface measurements.

Liu et al. [16] used a force sensitive wheeled probe to gather a rolling mechanical image to observe that a continuous measurement approach is more sensitive to differences in force profiles caused by simulated tumors than single-site data acquisition. However, rolling teeth cause periodic perturbations impairing the continuous measurement. An improved design by Liu et al. [15] with a greater complexity was able to identify spherical inclusions larger than 3 mm in diameter at a depth of less than 2 mm.

Non-contact sensing methods such as intraoperative MIS ultrasound probes [17] and optical coherence tomography (OCT) devices [36] have also been explored. These methods provide lower resolution compared to contact probes [14] and are limited to sensing within a comparatively low subcutaneous depth (0–2 mm).

Requirements for sterilization of devices are also essential considerations for the design of surgical tools [2]; heat, pressure, and humidity during treatment for tool reprocessing can destroy sensors. In the case of single-use devices a design for manufacturability in a sterile environment is required but considerations for reprocessing are circumvented. The simplicity of the design presented in this work allows for a low-cost single-use disposable.

Our Approach: While many of the tactile and force sensors described by Konstantinova et al. [14] have a subset of desired characteristics, limitations such as repeatability, ease of manufacturing, and cost, have slowed wide-spread adoption in clinical settings. Many of these sensors are often operable only in a discrete mode for orthogonal point measurements and cannot survive sterilization. As concluded by [14], “A number of devices have been developed to provide accurate tactile information during static measurements from one point. However, to detect information about mechanical properties of an organ, it is required to perform dynamic tissue scans.” There is a need for RMIS compatible sensors with rapid response time for stable measurements in

Property	Value
Probe-Tip Radius	2.25 mm
Force Resolution	4 mN
Maximum Linear Displacement	12 mm
Spring Rate	0.08 N/mm
Total Linear Offset of Device (from dVRK gripper)	75 mm
Magnetic Encoder	NSE5310
Pole Pair Length	2 mm
Number of Pole Pairs	6

TABLE I: Palpation Probe Specifications

sliding or rolling modes.

This paper presents a novel low-cost, single-use RMIS tool-tip deflection measurement device for localization of subcutaneous blood vessels. Our design achieves high speed sliding-mode palpation (tested up to 21 mm/s) while maintaining high sensitivity in deflection ($\sim 50 \mu\text{m}$) and force (4mN least count). Our palpation probe measures displacement-based force properties of tissue using a commercially available MEMS-based Hall Effect encoder as its core sensor. Hall Effect sensors measure minute changes in electric potential produced by magnetic flux passing through a conductor; a single sensor design favorably reduces fabrication complexity [14]. We use a 4.5 mm diameter spherical probe tip as the end-effector for tangential sliding point-contact interaction analogous to human fingertip palpation.

III. PALPATION PROBE DESIGN

A. Design Requirements

In addition to considerations for achieving high sensitivity at low-cost, the following issues were addressed:

1) *Compact Size and Low Cost*: The probe must match size constraints imposed by minimally invasive tools (diameter 5 mm to 12 mm) [18] used in laparoscopic procedures. The palpation probe was designed to mount onto the 8 mm diameter tool-tip of the da Vinci Research Kit (dVRK) Patient Side Manipulator (PSM). The current prototype adds a total length offset of 75 mm to the needle driver tool as shown in Figure 3. To limit costs, the probe sensing element is designed as a single-use add-on to an existing gripping tool. The gripper and data collection board may be reused.

2) *Resolution in Deflection*: Palpation measurements are improved by matching the impedance of test probe to sampled tissue. If the sensor is excessively stiff there would not be a measurable deflection in the probe tip to register an inclusion. If the sensor is too pliable tissue inclusions would not be registered as probe tip deflections. While searching for subcutaneous inclusions, it is essential to indent appreciably within tissue to observe a deflection in the probe, as demonstrated later in the experiments (see Figure 7(c)). The total displacement of the device was designed to be 10 mm with replaceable springs to allow for operation over tissues of different stiffness values.

B. Principle of Operation

The probe uses an end-effector with a known spring constant ($k = 0.08 \text{ N/mm}$) and Hall Effect sensing to compare displacement from the palpation probe to a known

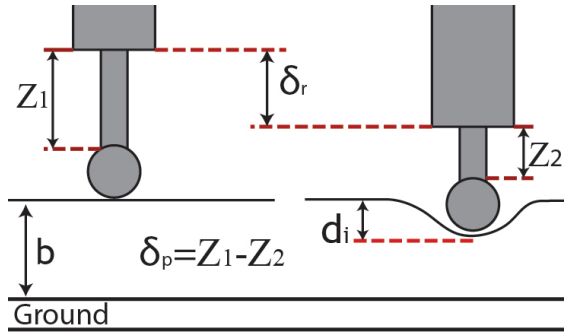


Fig. 2: A schematic illustrating the indentation process as well as the parameters which define the relationship between indentation depth and probe-tip deflection as described in Section III-B.

deflection value taken from a relative sample. The probe-tip displacement (δ_p) relative to the body of the device is measured with an incremental magnetic encoder and can be linearly related to a tissue reaction force (F) using Hooke's Law ($F = k\delta_p$).

For this device the indentation depth d_i can be calculated from the relative positions of the device (position of the robot arm), end effector (displacement of probe tip), and the baseline height (b) as (see Figure 2):

$$\begin{aligned}\delta_p &= Z_1 - Z_2 \\ d_i &= \delta_r - (\delta_p - b)\end{aligned}\quad (1)$$

where d_i is the depth of indentation, δ_p is the probe-tip displacement, δ_r is the displacement of the palpation probe body along the contact normal with respect to datum, and b is the baseline height of the sample.

IV. SYSTEM DESIGN

A. Sensing

Deflection of the probe tip was measured with an NSE5310 Austria Microsystems incremental position sensor. Magnetic Hall Effect sensors (such as the NSE5310) do not require direct contact with the sensed element which minimizes friction between the probe tip and the body of the device. The probe tip and axisymmetric magnet column were free to rotate with respect to the shaft of the da Vinci robot allowing the palpation probe to slide and rotate while in contact with surfaces. The NSE5310 magnetic encoder was mounted on the reverse of the electronics board and was located 0.125 mm from a central column of magnets which followed the movement of a 2.25 mm radius spherical indenter. Neodymium disc magnets (of 2 mm diameter and 2 mm pole pair length) were installed within the sense column with an inter-magnet air-gap of 2 mm. There were 4 magnets within the central column yielding a theoretical total displacement of 16 mm. Hard-stops were placed on the device to limit total displacement to 12 mm. The central column was made from magnetically permeable 316 Stainless Steel with a wall thickness of 0.23 mm and slid co-axially within 316 Stainless Steel bushings. Magnetic permeability is critical for allowing lines of flux to pass through the magnetic column to the NSE5310 Hall Effect sensors. An internal view of the mechanical components can be seen in Figure 3a.

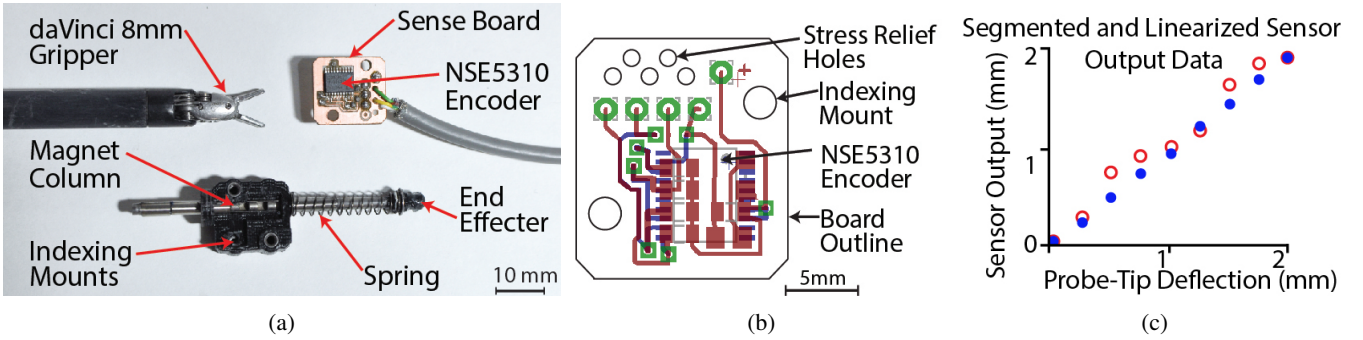


Fig. 3: An exploded view of palpation probe components. (a) Internal components of the probe with 8 mm da Vinci needle driver for comparison. The mounting bracket for the sensor is not shown. (b) Two layer printed circuit board design of the Sense Board showing surface mount components on top layer in red and bottom layer in blue. Connectors have been omitted from the design in the interest of minimizing size. (c) Linearization of output: Raw output of the sensor with respect to actual probe-tip position shown as red circles, cleaned data with non-linearities removed in real time signal processing as described in Section IV-C are shown in solid blue.

B. Electronics Design

To reduce size and cost, only components critical to sensing and voltage stability were included on-board the sensor. The power supply for the NSE5310 encoder was buffered and isolated using low-pass capacitors. A power indication LED and a current limiting 470Ω resistor were included for debugging. The total footprint of the electronics board is less than 15 mm per edge as illustrated in Figure 3b.

C. Signal Processing and Data Linearization

An Arduino Mega microprocessor was used for signal processing, data transmission, and interfacing with the dVRK. The NSE5310 encoder transmits 14-bit position measurements to the Arduino via I2C at a rate of 300Hz. A 50 sample sliding average low-pass filter was used to condition the raw encoder measurements.

Absolute position between magnet pole-pairs was calculated as a 14-bit integer in software by comparing any two consecutive readings and shifting the most significant bit up or down by one if the differences between consecutive readings was greater or less than a shifting threshold of 4000 or -4000 respectively. The shifting threshold was chosen to be greater than 6 standard deviations of noise away from the maximum sensor value of 4096 (sensor noise is addressed below).

Sensor output was recorded at known probe-tip indentation depths by mounting the sensor in a computer numerical controlled (CNC) Bridgeport vertical milling machine, as shown in Figure 5, equipped with a digital readout and accurate to 0.01 mm. For every probe-tip position, 10,000 samples were collected and averaged. These data points revealed a non-linearity between probe output and CNC measured compression as illustrated in Figure 3c. Transitional air gaps between magnetic pole-pairs, spaced alternately every 2 mm as seen in the *Magnet Column* in Figure 3a, create non-linearities in magnetic flux along the axis of travel. A six degree polynomial was fit to the 4 mm repeating segment of data used by the microprocessor to scale probe-tip indentation depth to a linear output as shown in Figure 3c.

D. Cost Estimates

The total cost for the electronics on the disposable printed circuit board was less than \$7.00 at the single-unit prototype scale. The structural hardware can be injection molded or made from simple tubular components and modular springs and cost less than \$2.00. The magnets used cost approximately \$0.01 each.

V. EXPERIMENTS AND dVRK INTEGRATION

A. Tissue Phantom with Linear Vessels

A tissue phantom comprising a cutaneous layer with subcutaneous inclusions was created for testing and characterization of the stiffness probe, as shown in Figure 4. Silicone Rubber *Ecoflex 00-30 (Smooth-On)* was cast in a 1A:1B ratio into a 100 mm long, 50 mm wide, 20 mm thick mold CNC machined from a block of *Delrin* to create a subcutaneous tissue matrix. Linear cylindrical inclusions of Silicone Rubber (thickness {1.58, 2.38, 3.175, 4.75} mm; Shore hardness of 70A) were arranged in the bottom of the mold prior to casting to serve as subcutaneous blood vessel phantoms. After setting, the subcutaneous phantom was unmolded and inverted. A cutaneous phantom was created using a slightly stiffer (shore harness 2A) *DragonSkin 10 Medium Silicone Rubber (Smooth-On)* in a 1A:1B ratio. Opaque pigmentation was achieved using a 0.5% by volume addition of Oil Pigment (Winton Oil Colour, Flesh Tint). The pigmented dermal layer was cast at various thicknesses ({1, 2, 3, 5} mm) in molds milled from *Delrin* (with width of 60 mm and length of 100 mm). Upon solidification, the dermal phantom was overlaid on the subcutaneous phantom (as shown in Figures 1) to create the tissue phantom setup.

B. Calibration using CNC Tool

The probe was affixed to a *Bridgeport* CNC vertical mill (with digital encoders accurate to 0.01 mm) for sensor calibration similar to the linearization procedure in Section IV-C. The tissue phantom was mounted securely to an acrylic plate affixed in a vise. The vertical position of the sensor was held constant at an initial probe deflection of 2 mm while the tissue phantom along with a cutaneous layer (lubricated by petroleum jelly) was moved beneath the sensor at a feed

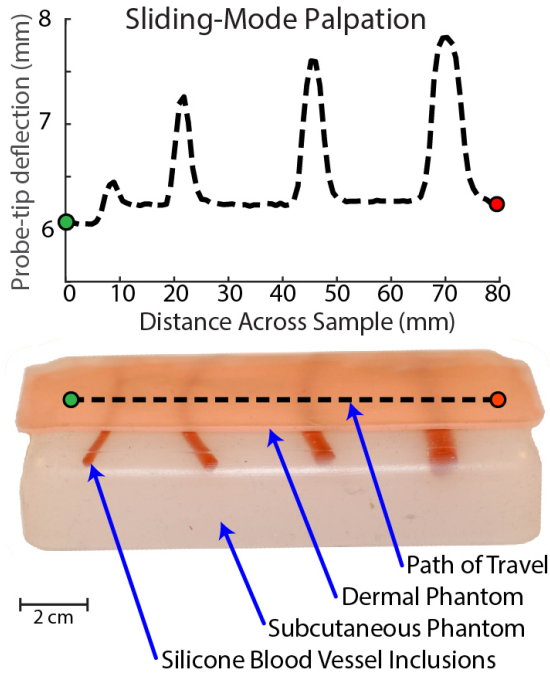


Fig. 4: A silicone tissue phantom is shown with blood vessel inclusions and overlaid dermal phantom. Sliding-mode palpation from starting point (green circle) to end point (red circle) over 80 mm of travel reveals the presence of subcutaneous blood-vessel inclusions as observed from the probe-tip deflection in the graph above. Depth of indentation was held constant at 8 mm, sliding speed was 1 mm/s, and skin thickness was 1 mm.

rate of 1 mm/s. Each trial was conducted across the same line running transverse to the veins embedded in the tissue phantom as shown in Figure 4. The standard error across 10 trials, quantified by normalized root mean square difference, was found to be $0.931 \mu\text{m}$.

Baseline sensor noise data ($> 10,000$ samples) were collected with no signal processing; the standard deviation of the noise was found to be $12.9 \mu\text{m}$. A measured value $52 \mu\text{m}$ ($\sim 4\sigma$) above baseline can be considered statistically dissimilar from noise; and using $F = k\delta_p$, we can get a minimum palpation probe sensitivity of 4 mN.

C. Probe Characterization using CNC Tool

A surface profile was constructed by interpolating the δ_p position of probed surface contact points spaced at 10 mm intervals along areas of interest. A surface contact point is described as the first time the probe registers a non-trivial measurement upon touching the surface; quantitatively defined as the δ_r position of the sensor after statistically significant deflection ($4\sigma \approx 52 \mu\text{m}$) is observed at the probe-tip (δ_p). This profile accounts for physical irregularities in the sample surface shape and is used to account for surface offset represented by b in Equation 1.

Figure 4 shows the probe-tip deflection (δ_p) using a sliding-mode measurement across the silicone tissue phantom with blood vessel phantoms and overlaid dermal phantom. The probe was slid across the surface from the starting point (green circle) to end point (red circle) over 80 mm of displacement. Parameters used in this trial were: indentation

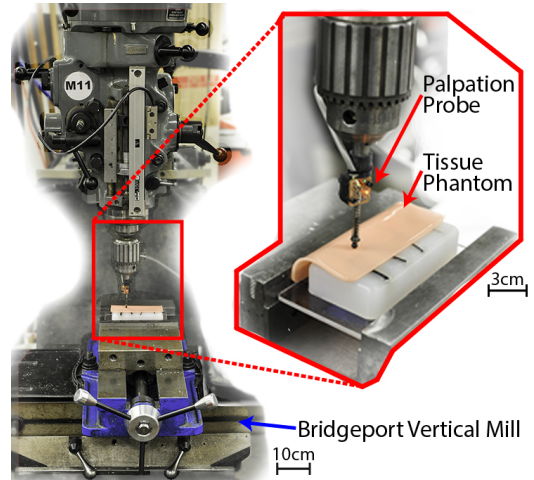


Fig. 5: Probe characterization on a Bridgeport CNC (XY-Axis) Vertical Mill. The vertical axis movement (δ_r in Equation 1) was measured by a digital encoder (accurate to 0.01 mm). For every setting of indentation depth, the vertical position was held constant as the tissue phantom was moved along a linear path across the subcutaneous vessels.

depth (δ_r) of 8 mm, sliding speed of 1 mm/s, and a skin thickness of 1 mm.

Deflection Response Characterization: Localization of a subcutaneous blood vessel (or tumor) depends on several parameters such as the *indentation depth*, *depth of the vessel* below the surface, and *speed of probe sliding*. Characterization of the probe behavior is essential to analyze the deflection response for different parameter settings.

Probe response was tested by varying each of these parameters for a fixed value of the other two as shown in the series of graphs in Figure 6. Each graph in the figure shows the variation in probe-tip deflection for different indentation depths (1 mm, 3 mm, 8 mm) at a fixed skin thickness and a constant sliding speed of 1 mm/s. The different graphs show the variation for different skin thicknesses (1 mm, 2 mm, 3 mm, 5 mm). Similarly, fixing the indentation depth at 8 mm and skin thickness at 1 mm, we varied the sliding speed to four different settings, ($\{0.5, 1, 6.3, 21\}$ mm/s) and observed the probing response as shown in Figure 7(a).

The probe was used to acquire deflection measurements along the same raster line in a forward and a backward pass. The results from this hysteresis analysis are shown in Figure 7(b); the maximum difference between the directional data was not statistically significant ($\geq 10 \times$ larger than 4σ of Gaussian noise).

D. dVRK Integration and Vein Localization

The palpation probe was mounted on the end of an 8 mm da Vinci Needle Driver as shown in Figures 1 and 9, extending the tool tip by 75 mm. Figure 7(c) shows the deflection response obtained for three indentation depths ($\{4, 6, \text{ and } 8\}$ mm) at 2 mm/s in single-sweep automated sliding-mode palpation.

An autonomous palpation routine was created for the dVRK accounting for the linear offset along the insertion direction as shown in Figure 8: a plane representing the

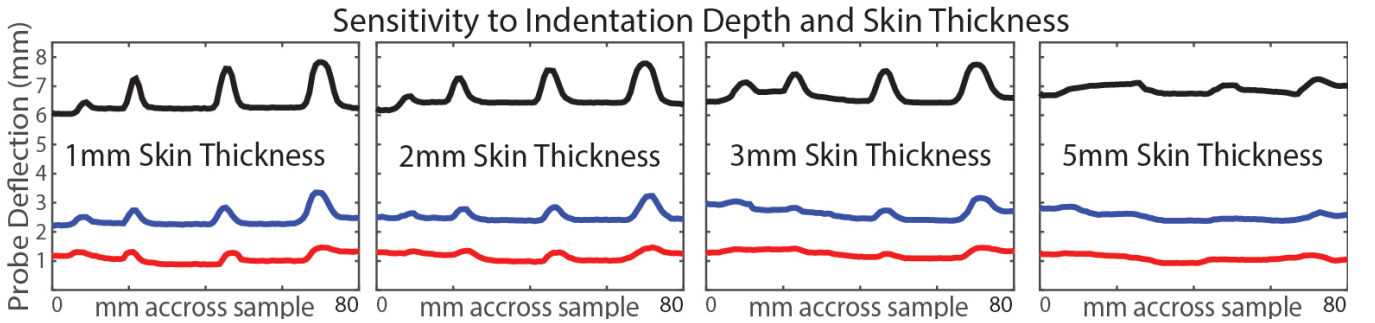


Fig. 6: Increasing Skin thickness decreases palpation probe sensitivity, while increasing penetration depth increases probe sensitivity to buried blood-vessel phantoms. Displacement of the probe-tip during sliding palpation plotted at 1 mm/s surface speed; indentation depth (δ_r) of 1 mm shown in red, 3 mm shown in blue, and 8 mm shown in black.

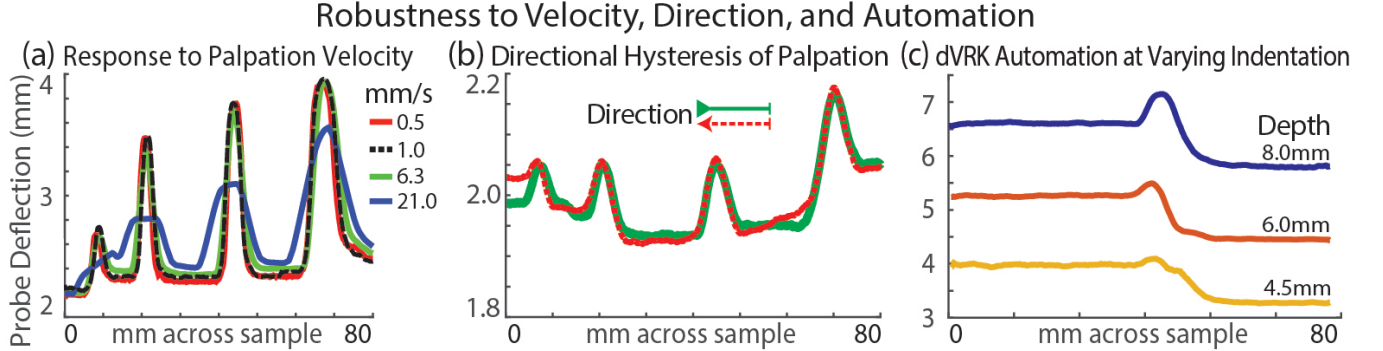


Fig. 7: Sensor response was tested with respect to varying speed, direction, and automation by the dVRK. (a) robustness to sliding speed was tested at four surface feed-rates; 0.5 mm/s is shown in red, 1 mm/s is shown in black, 6.3 mm/s is shown in green, and 21 mm/s is shown in blue. Probe indentation depth was held constant at 8 mm; skin thickness is 1 mm. (b) Hysteresis of sliding-mode palpation collected continuously in opposite directions without lifting the probe. The maximum maximum difference between data observed are within 4σ of noise levels, indicating very low hysteresis. Motion in the positive x-direction is shown in red; negative x-direction palpation is shown in green. This data was collected using a 1 mm skin thickness and 2 mm indentation at 1 mm/s sliding speed. (c) Deflection of palpation probe at three different indentation depths with an automated routine on the dVRK.

surface of the tissue phantom was created by recording the pose of the dVRK at the four corner points defined by point-contact of the palpation probe ($\geq 50 \mu\text{m}$ indentation). This plane ($45 \text{ mm} \times 25 \text{ mm}$) was segmented into 10 linear palpation sub-routines transversely crossing two subcutaneous blood vessel phantoms. The dVRK returned the palpation probe-tip to a home position 2cm above the area of interest between each linear segment. Continuous tangential palpation at 2 mm/s with an indentation depth of 8 mm was used to search within the area of interest on the tissue phantom. The blood vessel silicone phantoms used for these trials were 2.5 mm and 3.5 mm in diameter embedded subcutaneously beneath a layer of 1 mm thick dermal phantom. An estimate of the location of subcutaneous vessels generated by Delaunay interpolation of a raster scanning pattern is illustrated in Fig. 8. Start and end points of the raster path are shown overlaid above a tissue phantom as green and red circles respectively.

VI. DISCUSSION AND FUTURE WORK

A. Discussion of Results

Preliminary characterization results from the palpation probe demonstrate the ability to identify and localize a subcutaneous blood vessel. As observed in Figure 4, as the size of underlying vessel increases the sensor deflection also

increases. However, in all cases the deflection obtained is significantly above noise ($\geq 10 \times$ larger than 4σ of Gaussian noise). Increasing depth of the inclusion decreases the signal-to-noise ratio from 40:1 at 1 mm skin thickness to $\sim 4:1$ at 5 mm skin thickness for a vessel of diameter 4.75 mm. Signal-to-noise ratio amplifies approximately linearly with increase in indentation depth as observed in Figure 6. A discernible peak is obtained even in the raw data without signal conditioning for a subcutaneous vessel of 2.25 mm diameter under a 5 mm skin with an 8 mm indentation depth. As we increase the sliding speed of the probe on the phantom surface, we observe a small decrease in signal-to-noise ratios as shown in Figure 7(a). However, even the speed of 21 mm/s, which is comparatively high in context of RMIS, we obtain statistically significant deflections for all 4 subcutaneous vessels.

Repeatability in measurements is required of RMIS probes which is supported by measurements obtained from forward and backward runs of the probe along the same raster line. These measurements are within acceptable noise levels of $50 \mu\text{m}$ ($\approx 4\sigma$) as shown in Figure 7(b).

Experiments with autonomous palpation routines on dVRK corroborate the findings from probe characterization on CNC machine tool. In spite of the millimeter level positioning inaccuracies in the dVRK, Figure 7(c) shows a

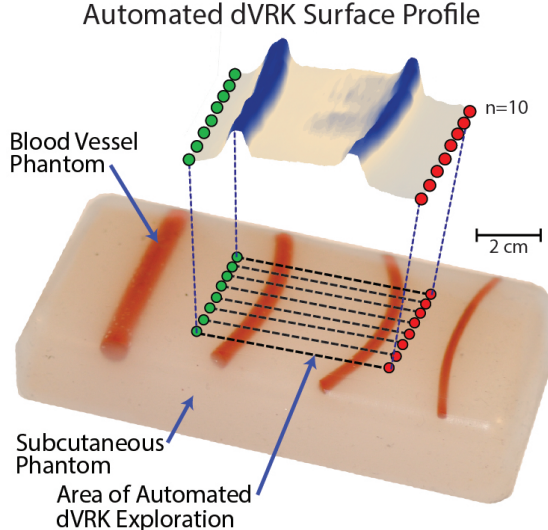


Fig. 8: An estimate of subcutaneous blood vessels generated by a raster scan on the region of interest. Delaunay surface interpolation was used to create a continuous estimate from raster samples. Start and end points for each linear segment are shown overlaid above a tissue phantom as green and red circles respectively with indicative raster scan paths (shown as black dashed lines).

high gain in signal with increase in indentation depth with constant skin thickness and sliding speed. Further, the raster scan results from Figure 8 demonstrate that this method can be used to search and localize a subcutaneous inclusion in a large surface area and can be automated for use by RMIS devices.

B. Future Work

The proposed sensor is primarily aimed to differentiate areas of interest based on relative deflection changes. However, the tool could provide estimated stiffness values using inverse calculations as in work by Yu et al. [35] and Hayes et al [12]. Also, the electronics board can be miniaturized further to fit within the cylindrical profile of the da Vinci's 8 mm Needle Driver by designing with smaller surface mount components and traces. Methods for noise reduction and signal amplification can extend the limits of the sensor to identify deeper inclusions while negating the effects of errors in robot positioning.

Autonomous palpation and localization can be improved with the use of active sensing algorithms. As an example, Nichols et al. [20] presented a probabilistic sensing algorithm which can be leveraged to enable autonomous searching within a target area. They used a 45 mm indentation ball which is limited to sensing large inclusions, while our probe would extend their work to a fine grained localization of smaller inclusions. Nichols et al. relied on point measurements, while our probe uses a sliding-mode continuous measurement. Information-gathering algorithms for autonomous localization of inclusions, such as the ones compared by Goldman et al. [10], may be considered for this continuous (sliding-mode) probe.

Previous works have not investigated methods for automated shape and impedance exploration in unknown flexible

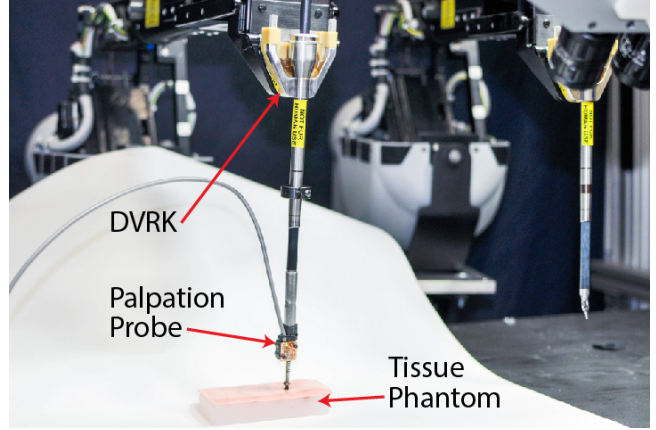


Fig. 9: The presented haptic palpation probe can be automated to search for blood vessel phantoms with the da Vinci Research Kit Patient Side Manipulator.

environments with a continuous probing mechanism. Possessing prior knowledge of the surface profile, the insertion axis of the dVRK could be used to maintain consistent probe-tip indentation depth across non-planar (or irregular) surface paths while searching tissue for inclusions.

VII. CONCLUSIONS

We have presented a novel low-cost, single-use palpation probe for usage with RMIS for localizing subcutaneous blood vessels and tumors. It senses relative differences in probe tip reaction force by measuring tip deflection with respect to a known spring constant using a Hall Effect sensor. The palpation probe fits on the end of a 8 mm diameter needle driver and extends it by 75 mm. It is an indentation based probe which can be used for quasi-static sliding palpation as well as for discrete point palpation. We have used discrete measurements for generating a surface profile of an unknown silicone tissue phantoms; quasi-static sliding was then used for identifying subcutaneous blood vessel phantoms. The issue of sterilization is circumvented by use of disposable sensors, wherein a cost of less than \$10 is achieved by use of off-the-shelf electronics and 3D printed components.

The sensor probe was characterized for deflection response on a CNC machine tool with respect to various parameter settings such as multiple diameters of subcutaneous silicone cylinders (1.58-4.75 mm) at varying subcutaneous depths (1-5 mm) with a range of indentation depths (0-8 mm) and sliding speeds (0.5-21 mm/s). Experiments with the dVRK under autonomous execution were also performed and suggest that probing routines could be automated adaptively in minimally invasive surgeries. The probe can detect subcutaneous structures in phantoms of diameter 2.25 mm at a depth of up to 5 mm below the tissue surface and can operate up to speeds of 21 mm/s in sliding-mode palpation.

The authors will extend this study to further miniaturize the sensor. Improvement in design of the probe tip mount on the tool to allow for wrist rotation to control sensor orientation is also envisioned. Finally the authors will leverage this device to autonomously palpate and localize

subcutaneous inclusions and extend this work to for an autonomous excision routine.

Acknowledgements

This work is supported in part by a seed grant from the UC Berkeley Center for Information Technology in the Interest of Science (CITRIS), and by the U.S. National Science Foundation under Award IIS-1227536: Multilateral Manipulation by Human-Robot Collaborative Systems. We thank Intuitive Surgical, and in particular Simon DiMao, for making the dVRK possible and the entire dVRK community for support; NVIDIA for computing equipment grant, and Sanjay Krishnan for the valuable feedback.

REFERENCES

- [1] K. Althoefer, D. Zbyszewski, H. Liu, P. Puangmali, L. Seneviratne, B. Challacombe, P. Dasgupta, and D. Murphy, "Air-cushion force sensitive probe for soft tissue investigation during minimally invasive surgery," in *Sensors, 2008 IEEE*. IEEE, 2008, pp. 827–830.
- [2] ST79-Comprehensive guide to steam sterilization and sterility assurance in health care facilities., ANSI/AAMI Std. ST79:2010/A4:2013.
- [3] M. Beccani, C. Di Natali, L. J. Sliker, J. A. Schoen, M. E. Rentschler, and P. Valdastri, "Wireless tissue palpation for intraoperative detection of lumps in the soft tissue," *Biomedical Engineering, IEEE Transactions on*, vol. 61, no. 2, pp. 353–361, 2014.
- [4] M. R. Cutkosky, R. D. Howe, and W. R. Provancher, "Force and tactile sensors," in *Springer Handbook of Robotics*. Springer, 2008, pp. 455–476.
- [5] S. A. Darzi and Y. Munz, "The impact of minimally invasive surgical techniques," in *Annu Rev Med.*, vol. 55, 2004, pp. 223–237.
- [6] B. Demi, T. Ortmaier, and U. Seibold, "The touch and feel in minimally invasive surgery," in *Haptic Audio Visual Environments and their Applications, 2005. IEEE International Workshop on*. IEEE, 2005, pp. 6–pp.
- [7] N. Futai, K. Matsumoto, and I. Shimoyama, "A flexible micromachined planar spiral inductor for use as an artificial tactile mechanoreceptor," *Sensors and Actuators A: Physical*, vol. 111, no. 2, pp. 293–303, 2004.
- [8] J. B. Gafford, S. B. Kesner, A. Degirmenci, R. J. Wood, R. D. Howe, and C. J. Walsh, "A monolithic approach to fabricating low-cost, millimeter-scale multi-axis force sensors for minimally-invasive surgery," in *Robotics and Automation (ICRA), 2014 IEEE International Conference on*. IEEE, 2014, pp. 1419–1425.
- [9] P. S. Girão, P. M. P. Ramos, O. Postolache, and J. M. D. Pereira, "Tactile sensors for robotic applications," *Measurement*, vol. 46, no. 3, pp. 1257–1271, 2013.
- [10] R. E. Goldman, A. Bajo, and N. Simaan, "Algorithms for autonomous exploration and estimation in compliant environments," *Robotica*, vol. 31, no. 01, pp. 71–87, 2013.
- [11] J. C. Gwilliam, Z. Pezzementi, E. Jantho, A. M. Okamura, and S. Hsiao, "Human vs. robotic tactile sensing: Detecting lumps in soft tissue," in *Haptics Symposium, 2010 IEEE*. IEEE, 2010, pp. 21–28.
- [12] W. Hayes, L. Keer, G. Herrmann, and L. Mockros, "A mathematical analysis for indentation tests of articular cartilage," *Journal of biomechanics*, vol. 5, no. 5, pp. 541–551, 1972.
- [13] Y. Hu, R. Katragadda, H. Tu, Q. Zheng, Y. Li, and Y. Xu, "Bioinspired 3-d tactile sensor for minimally invasive surgery," *Microelectromechanical Systems, Journal of*, vol. 19, no. 6, pp. 1400–1408, Dec 2010.
- [14] J. Konstantinova, A. Jiang, K. Althoefer, P. Dasgupta, and T. Nanayakkara, "Implementation of tactile sensing for palpation in robot-assisted minimally invasive surgery: A review," *Sensors Journal, IEEE*, vol. 14, no. 8, pp. 2490–2501, Aug 2014.
- [15] H. Liu, J. Li, X. Song, L. D. Seneviratne, and K. Althoefer, "Rolling indentation probe for tissue abnormality identification during minimally invasive surgery," *Robotics, IEEE Transactions on*, vol. 27, no. 3, pp. 450–460, 2011.
- [16] H. Liu, D. P. Noonan, B. J. Challacombe, P. Dasgupta, L. D. Seneviratne, and K. Althoefer, "Rolling mechanical imaging for tissue abnormality localization during minimally invasive surgery," *Biomedical Engineering, IEEE Transactions on*, vol. 57, no. 2, pp. 404–414, 2010.
- [17] G. L. McCreery, A. L. Trejos, M. D. Naish, R. V. Patel, and R. A. Malthaner, "Feasibility of locating tumours in lung via kinaesthetic feedback," *The International Journal of Medical Robotics and Computer Assisted Surgery*, vol. 4, no. 1, pp. 58–68, 2008.
- [18] D. McKay and G. Blake, "Optimum incision length for port insertion in laparoscopic surgery," *Annals of the Royal College of Surgeons of England*, vol. 88, no. 1, p. 78, 2006.
- [19] Y. Murayama, M. Haruta, Y. Hatakeyama, T. Shiina, H. Sakuma, S. Takenoshita, S. Omata, and C. E. Constantinou, "Development of a new instrument for examination of stiffness in the breast using haptic sensor technology," *Sensors and Actuators A: Physical*, vol. 143, no. 2, pp. 430–438, 2008.
- [20] K. A. Nichols and A. M. Okamura, "Methods to segment hard inclusions in soft tissues," *IEEE Transactions on Robotics*, accepted.
- [21] M. Ohka, N. Morisawa, H. Suzuki, J. Takata, H. Koboyashi, and H. Yussof, "A robotic finger equipped with an optical three-axis tactile sensor," in *Robotics and Automation, 2008. ICRA 2008. IEEE International Conference on*, May 2008, pp. 3425–3430.
- [22] K. Ohuchida and M. Hashizume, "Robotic surgery for cancer," *The Cancer Journal*, vol. 19, no. 2, pp. 130–132, 2013.
- [23] P. Peng and R. Rajamani, "Handheld microtactile sensor for elasticity measurement," *Sensors Journal, IEEE*, vol. 11, no. 9, pp. 1935–1942, 2011.
- [24] P. Puangmali, K. Althoefer, L. D. Seneviratne, D. Murphy, and P. Dasgupta, "State-of-the-art in force and tactile sensing for minimally invasive surgery," *Sensors Journal, IEEE*, vol. 8, no. 4, pp. 371–381, 2008.
- [25] M. Qasaimeh, S. Sokhanvar, J. Dargahi, and M. Kahrizi, "Pvdf-based microfabricated tactile sensor for minimally invasive surgery," *Microelectromechanical Systems, Journal of*, vol. 18, no. 1, pp. 195–207, Feb 2009.
- [26] A. Sarvazyan, "Computerized palpation is more sensitive than human finger," in *Proceedings of the 12th International Symposium on Biomedical Measurements and Instrumentation*, 1998, pp. 523–24.
- [27] A. Shashank, M. Tiwana, S. Redmond, and N. Lovell, "Design, simulation and fabrication of a low cost capacitive tactile shear sensor for a robotic hand," in *Engineering in Medicine and Biology Society, 2009. EMBC 2009. Annual International Conference of the IEEE*, Sept 2009, pp. 4132–4135.
- [28] H. Takao, K. Sawada, and M. Ishida, "Monolithic silicon smart tactile image sensor with integrated strain sensor array on pneumatically swollen single-diaphragm structure," *Electron Devices, IEEE Transactions on*, vol. 53, no. 5, pp. 1250–1259, 2006.
- [29] S. Takenawa, "A soft three-axis tactile sensor based on electromagnetic induction," in *Mechatronics, 2009. ICM 2009. IEEE International Conference on*, April 2009, pp. 1–6.
- [30] M. I. Tiwana, S. J. Redmond, and N. H. Lovell, "A review of tactile sensing technologies with applications in biomedical engineering," *Sensors and Actuators A: Physical*, vol. 179, pp. 17–31, 2012.
- [31] A. L. Trejos, J. Jayender, M. Perri, M. D. Naish, R. V. Patel, and R. Malthaner, "Robot-assisted tactile sensing for minimally invasive tumor localization," *The International Journal of Robotics Research*, 2009.
- [32] R. Veldkamp, E. Kuhry, W. Hop, J. Jeekel, G. Kazemier, H. J. Bonjer, E. Haglind, L. Pahlman, M. A. Cuesta, S. Msika *et al.*, "Laparoscopic surgery versus open surgery for colon cancer: short-term outcomes of a randomised trial," *Lancet Oncol*, vol. 6, no. 7, pp. 477–484, 2005.
- [33] S. K. Venkatesh, M. Yin, J. F. Glockner, N. Takahashi, P. A. Araoz, J. A. Talwalkar, and R. L. Ehman, "Magnetic resonance elastography of liver tumors-preliminary results," *AJR. American Journal of Roentgenology*, vol. 190, no. 6, p. 1534, 2008.
- [34] S. B. Williams, M.-H. Chen, A. V. D'Amico, A. C. Weinberg, R. Kacker, M. S. Hirsch, J. P. Richie, and J. C. Hu, "Radical retropubic prostatectomy and robotic-assisted laparoscopic prostatectomy: likelihood of positive surgical margin (s)," *Urology*, vol. 76, no. 5, pp. 1097–1101, 2010.
- [35] W. Yu, Y. Li, Y. Zheng, N. Lim, M. Lu, and J. Fan, "Softness measurements for open-cell foam materials and human soft tissue," *Measurement Science and Technology*, vol. 17, no. 7, p. 1785, 2006.
- [36] A. M. Zysk, F. T. Nguyen, A. L. Oldenburg, D. L. Marks, and S. A. Boppart, "Optical coherence tomography: a review of clinical development from bench to bedside," *Journal of Biomedical Optics*, vol. 12, no. 5, pp. 051403–051403, 2007.